Supporting Information

The role of stoichiometry in the growth of large $Pb_2P_2Se_6$ crystals for nuclear radiation detection

Yadong Xu[†, ‡], Xu Fu[†], Hongjian Zheng[†], Yihui He[‡], Wenwen Lin[‡], Kyle M. McCall[‡, §], Zhifu Liu[§], Sanjib Das[§], Bruce W. Wessels[§], Mercouri G. Kanatzidis[‡, §]

[†]State Key Laboratory of Solidification Processing, Northwestern Polytechnical University, Xi'an 710072, China,
[‡]Department of Chemistry, Northwestern University, Evanston, IL 60208
[§]Department of Materials Science and Engineering, Northwestern University, Evanston, IL 60208

S1: Optical and SEM+EDS Measurements

As-grown $Pb_2P_2Se_6$ wafers cut from the different ingots were evaluated by IR and optical transmission microscopy, as seen in Figure S1. The resulting high-contrast IR images were obtained due to the strong absorption or scattering of the secondary phase (SP) particles. In these images, the distinct dark areas are associated with the presence of SP particles in the $Pb_2P_2Se_6$ wafer.
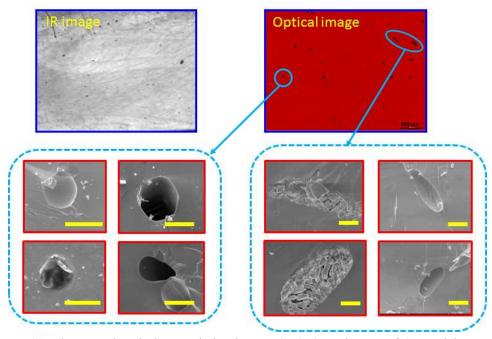

Figure S1. The IR and optical transmission images (top), SEM images of SP particles on the $Pb_2P_2Se_6$ crystal surface (bottom), all scale bars correspond to 20 μm.

To reduce the impact of surface processing and avoid surface contamination, pristine $Pb_2P_2Se_6$ crystals were cleaved for scanning electron microscopy studies of the SP particle's morphology, Figure S1 (bottom). Simultaneously, the chemical composition of local areas in $Pb_2P_2Se_6$ samples was determined by the EDS analysis, as shown in Figure S2.
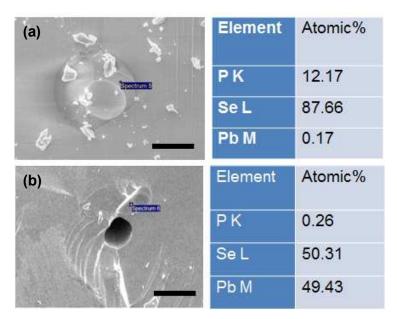
(a)	Element	Atomic%
	P K	12.17
	Se L	87.66
	Pb M	0.17

(b)	Element	Atomic%
	P K	0.26
	Se L	50.31
	Pb M	49.43

Figure S2. The SEM images of SP inclusions embedded in $Pb_2P_2Se_6$ crystal, and corresponding EDS analysis, (a) P-Se SP in Se-rich crystal, (b) Pb-Se SP in Pb-rich crystal, all scale bars correspond to 20 μm.

S2: Calculation Method Summary

We calculate the defect formation energy for the charge state q dependent on the Fermi level position according to[1,2]

$$E_f[X^q] = E^{tot}[X^q] - E^{tot}[bulk] - \sum_i n_i u_i + q(E_F + E_v + \Delta V) + E_{corr} \quad (1)$$

Where $E^{tot}[X^q]$ is the total energy derived from a supercell with defect X and charge q, and $E^{tot}[bulk]$ is the total energy for the perfect crystal using an equivalent supercell, n_i is the number of atoms of type i that has been added to ($n_i > 0$) or removed ($n_i < 0$) from the supercell to form the defect, and u_i is the corresponding chemical potential of the specie. E_F is the Fermi level with respect to the bulk valence-band maximum (VBM) E_v, and ΔV is a correction term to align the reference potential in our defect supercell to that in the bulk.

E_{corr} is a correction term due to the presence of periodic images, which can correct the finite-size error that arises from the electrostatic interaction between charged defects in neighboring cell images. There are several schemes that have been proposed to correct this error.[3-5] In this paper, the correction term suggested by Freysoldt *et. al.* is adopted,[4] which uses a planar average of the electrostatic short range potential and works well for the small relaxation.

The thermodynamic transition level $\varepsilon(q_1/q_2)$ is defined as the Fermi-level position for which the formation energies of charge states q_1 and q_2 are equal:

$$\varepsilon(q_1/q_2) = \frac{E^f(X^{q_1}; E_f=0) - E^f(X^{q_2}; E_f=0)}{q_2 - q_2} \tag{2}$$

Where $E^f(X^{q_1}; E_f = 0)$ is the formation energy of the defect X in the charge state q when the Fermi level is at the VBM (E_F=0). The significance of this level is that charge state q_1 is stable for Fermi-level positions below $\varepsilon(q_1/q_2)$ while charge state q_2 is above $\varepsilon(q_1/q_2)$.

According to Eq. (1), we can find the defect formation energy also depends on chemical potentials u_X. In the case of the ternary P-Pb-Se system, the u_X (X = P, Pb, Se) values are determined from the equilibrium conditions of various phases containing P, Pb, and Se. Figure. S3 shows the schematic phase diagram of the ternary system P-Pb-Se [6, 7]. Thus, the chemical potentials of the three elements can vary in the following correlation from Eq. (3) to Eq. (6).
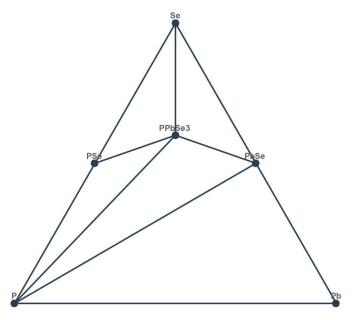

Figure S3. Schematic phase diagram of the P-Pb-Se ternary system.

$$u_P + u_{Pb} + \mu_{Se} = u_{PPbSe3\,(bulk)} \tag{3}$$

$$\mu_{Pb} + \mu_{Se} = \mu_{PbSe}\ (bulk) \tag{4}$$

$$\mu_P + \mu_{Se} = \mu_{PSe(bulk)} \tag{5}$$

$$\mu_P \leq \mu_{P(bulk)},\ \mu_{Pb} \leq \mu_{Pb(bulk)},\ \mu_{Se} \leq \mu_{Se(bulk)} \tag{6}$$

The formation energies of all the stable phases from Materials Project[6,7] are listed

in Table. S1.

Table. S1 Formation energies of all the stable phases in P-Pb-Se system.

Formula	P	Pb	Se	PSe	PbSe	PPbSe$_3$
Formation Energy/Atom (eV)	0	0	0	-0.08	-0.57	-0.468

Considering the Se- and Pb-saturated conditions, the corresponding chemical potential is demonstrated in Table S2 and Table S3, respectively.

Table. S2 Chemical potential of the Se-PSe system.

Element	P	Pb	Se
Potential/eV	-5.56	-5.13	-3.49

Table. S3 Chemical potential of the PbSe-P system.

Element	P	Pb	Se
Potential/eV	-5.41	-4.60	-3.73

S3: TSC Results Calculation Summary

The characterization of deep traps means the determination of their main parameters ('trap signatures'), particularly the thermal activation energy (E_a) and concentration (N), to understand their effects on the electrical characteristics of semi-insulating materials.

Since the current peaks formed by the release of trapped carriers in defect levels always overlap with each other, the simultaneous multiple peak analysis (SIMPA) method,[8] based on the "first order kinetics" approximation, was adopted to determine trap signatures in TSC spectra. A single TSC peak resulting from an electron trap can be described as

$$I_{TSC}^i(T) = N_{Ti}\mu_n\tau_n eAED_{t,i}T^2 \exp\{-\frac{E_{a,i}}{kT} - \frac{kD_{t,i}}{\beta E_{a,i}}T^4 \times \exp(-\frac{E_{a,i}}{kT})$$
$$\times [1 - 4\frac{kT}{E_{a,i}} + 20(\frac{kT}{E_{a,i}})^2]\}$$

(7)

Where, e is the electron charge, μ is the carrier mobility, τ is the carrier lifetime, A is the area of the electrode, E is the applied electric field, k is the Boltzmann constant, T is the absolute temperature and β is the heating rate. $E_{a,i}$ is the thermal activation energy of the ith trap which is related to the TSC peak position. $D_{t,i}$ is a temperature and trap dependent coefficient and is defined as $D_{t,i} = 3\times10^{21}(m^*/m^0)\sigma_i$, where m^0 and m^* represent the electron (or hole) rest and effective masses, respectively.

In our TSC results calculations, the $\mu\tau$ product at 300 K was taken to be 10^{-5}

$cm^2 \cdot V^{-1}$, corresponding to the value estimated from previous measurements. The heating rate was set as 0.2 K/s. The area of the electrode and the applied electric field were measured to be ~0.01cm^2 and 50 V/cm. The m^*/m^0 ratio is taken to be 0.3 according to data from Ref. [9]
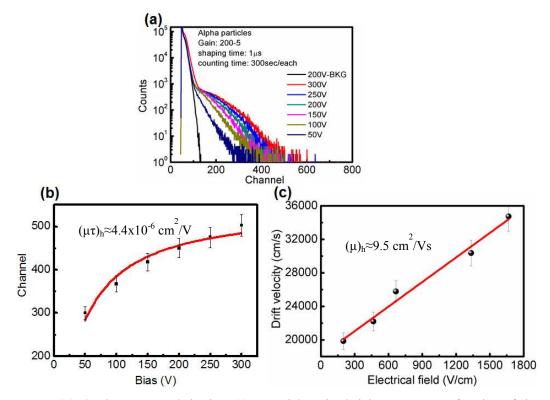
S4: Alpha Particle response

Figure S4. Carrier transport behaviors (a) α particle pulse height spectra as a function of the applied bias. (b) $(\mu\tau)_h$ of Pb-rich $Pb_2P_2Se_6$ fitted using the single carrier Hecht equation. (c) Holes drift velocity as a function of the electrical field strengths of Pb-rich $Pb_2P_2Se_6$.

S5: Gamma-ray and X-ray Detector Performance

Planar-type $Pb_2P_2Se_6$ detectors were prepared, where the C or Au electrodes were on parallel surfaces of the crystal. Carbon electrodes were prepared by depositing colloidal graphite paint, and Au contacts were deposited by thermal evaporation. Uncollimated 0.2 mCi ^{57}Co @ 122 keV and 1 μCi ^{241}Am @ 59.5 keV γ-ray sources were employed to irradiate the samples. In each measurement, the as-prepared detectors were placed in an enclosed shielding box under cathode irradiation at room temperature.

Current voltage (I/V) measurements were performed on planar deices. The current

dependent I/V curves were investigated in the X-ray tube current range from 5 μA to 100 μA and a tube bias of 40 kVp using a Keithley 6517b picoammeter/voltage supply.
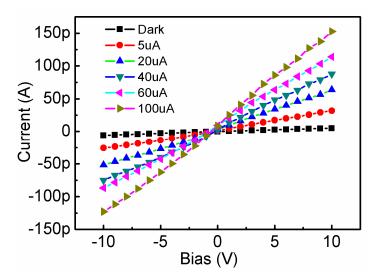

Figure S5. I-V characteristics of Pb-rich $Pb_2P_2Se_6$ sample in darkness and under different X-ray illumination (tube bias of 40 kVp, and tube current is in the range of 5-100 μA).

REFERENCES

(1) Van de Walle C G.; Neugebauer J. First-principles calculations for defects and impurities: Applications to III-nitrides. *J. Appl. Phys*. **2004**, 95(8): 3851-3879.

(2) Freysoldt C.; Grabowski B.; Hickel T.; et al. First-principles calculations for point defects in solids. *Rev. Mod. Phys*. **2014**, 86(1): 253.

(3) Makov G.; Payne M C. Periodic boundary conditions in ab initio calculations. *Phys. Rev. B*, **1995**, 51(7): 4014.

(4) Freysoldt C.; Neugebauer J.; Van de Walle C G. Fully ab initio finite-size corrections for charged-defect supercell calculations. *Phys. Rev. Lett*. **2009**, 102(1), 016402.

(5) Kumagai Y.; Oba F. Electrostatics-based finite-size corrections for first-principles point defect calculations. *Phys. Rev. B*, **2014**, 89(19), 195205.

(6) Ping S.; Wang L.; Kang B.; et al. Li- Fe- P-O2 phase diagram from first principles calculations. *Chemistry of Materials*, **2008**, 20(5), 1798-1807.

(7) Jain A.; Hautier G.; Ong S P.; et al. Formation enthalpies by mixing GGA and GGA+ U calculations. *Phys. Rev. B*, **2011**, 84(4), 045115.

(8) Pavlovic M.; and Desnica U. V. Precise determination of deep trap signatures and their relative and absolute concentrations in semi-insulating GaAs. *J. Appl. Phys*. **1998**, 84(4), 2018-2024.

(9) Kostina S. S.; Hanson P.; Wang P.; Peters J.; Valverde-Chavez D.; Chen P.; Cooke D.; Kanatzidis M.; and Wessels B. Charge transport mechanisms in a $Pb_2P_2Se_6$ semiconductor. *ACS Photonics*, **2016**, 3, 1877-1887